

A.A. KOSTEREV<sup>1,✉</sup>  
F.K. TITTEL<sup>1</sup>  
W. DURANTE<sup>2</sup>  
M. ALLEN<sup>3</sup>  
R. KÖHLER<sup>4,\*</sup>  
C. GMACHL<sup>4</sup>  
F. CAPASSO<sup>4</sup>  
D.L. SIVCO<sup>4</sup>  
A.Y. CHO<sup>4</sup>

## Detection of biogenic CO production above vascular cell cultures using a near-room-temperature QC-DFB laser

<sup>1</sup> Rice Quantum Institute, Rice University, Houston, TX 77 251-1892, USA

<sup>2</sup> Departments of Medicine and Pharmacology, Baylor College of Medicine, Houston, TX 77 030, USA

<sup>3</sup> Physical Sciences Inc., 20 New England Business Center, Andover, MA 01810, USA

<sup>4</sup> Bell Laboratories, Lucent Technologies, 600 Mountain Avenue, Murray Hill, NJ 07974, USA

Received: 24 October 2001

Published online: 29 November 2001 • © Springer-Verlag 2001

**ABSTRACT** We report the first application of pulsed, near-room-temperature quantum cascade laser technology to the continuous detection of biogenic CO production rates above viable cultures of vascular smooth muscle cells. A computer-controlled sequence of measurements over a 9-h period was obtained, resulting in a minimum detectable CO production of 20 ppb in a 1-m optical path above a standard cell-culture flask. Data-processing procedures for real-time monitoring of both biogenic and ambient atmospheric CO concentrations are described.

PACS 42.62.Be; 82.80.Gk

### 1 Introduction

The role of simple molecules such as nitric oxide (NO) in physiological processes has received considerable attention in recent years and was a subject of the 1998 Nobel Prize in Medicine. Recent work indicates that other gases, such as carbon monoxide (CO), can also play a very significant role as a physiological messenger – similar to that of NO. CO is produced from heme catabolism by the enzyme heme oxygenase. Previous work has shown that CO promotes blood flow by inhibiting vascular tone and platelet aggregation [1] and that neuronal CO production may modulate the NO-cGMP (guanosine 3', 5'-cyclic monophosphate) signaling system, demonstrating important biochemical interactions between these two diatomic gases. The extremely low levels of gas production in living cells and the relatively short in vitro lifetime of cell cultures have complicated detailed understanding of the kinetic or time-dependent processes responsible for their generation. A typical production rate of CO, for example from vascular smooth muscle cells (VSMCs), is 1 to 10 pmol/min/10<sup>7</sup> cells. Instrumentation for in vitro measurement of gas production should have sensitivities on the parts per billion (ppb) level so that the dynamics of gas production can be followed with laboratory-scale cell sample populations [2].

Because of this low production rate from biological tissues, measurements of CO concentrations have been limited to gas chromatography [3–5] and radioisotope counting [6] techniques. Although these methods are highly sensitive, they cannot measure CO directly, requiring several time-consuming intermediate steps (~15 min), and may be affected by interference from water, oxygen, and carbon dioxide.

Infrared laser absorption spectroscopy is an attractive alternative approach for the detection of biological CO at the parts per billion level in real time. In [7], endogenous CO production from vascular cells was measured by using a mid-IR laser based on difference-frequency generation (DFG) of two near-IR lasers as a spectroscopic source. The CO absorption was detected in the fundamental vibration band near 4.6  $\mu\text{m}$ . In that work, an extractive technique was used with gas samples taken from the flask containing the cell culture to an 18-m-path-length optical multipass cell so that the measurements could be performed at a reduced pressure of 100 Torr.

In this paper we report an improved design and performance of an optical mid-IR CO sensor intended for in vitro, continuous monitoring of cell-culture activity at ambient atmospheric pressure. The same fundamental absorption-band region was used for CO detection, but a quantum cascade laser with a distributed feedback structure (QC-DFB) [8] was employed instead of the DFG source. The high output power of the QC-DFB laser and an advanced data-analysis approach made it possible to detect biological CO and CO production rates with ~1-m optical path length folded above a standard culture flask of VSMCs.

### 2 Experimental setup

The measurements of CO concentration above cell cultures were completed using the optical configuration shown in Fig. 1. The pulsed QC-DFB laser was mounted on a three-stage thermoelectric cooler inside a vacuum-tight housing sealed with a 30' wedged uncoated CaF<sub>2</sub> window. Laser radiation was collimated with an aspheric ZnSe lens ( $f = 3$  mm, 6-mm diameter) positioned inside the housing. The output of the laser was split into signal and reference beams using an uncoated ZnSe wedge. The main beam was folded into a sealed vessel containing the cell-culture flask, a temperature-stabilized surface for maintaining the cells at an elevated temperature of +37 °C, and three flat mirrors.

✉ Fax: +1-713/348-5686, E-mail: akoster@rice.edu

\*Present address: Scuola Normale Superiore, Pisa, Italy

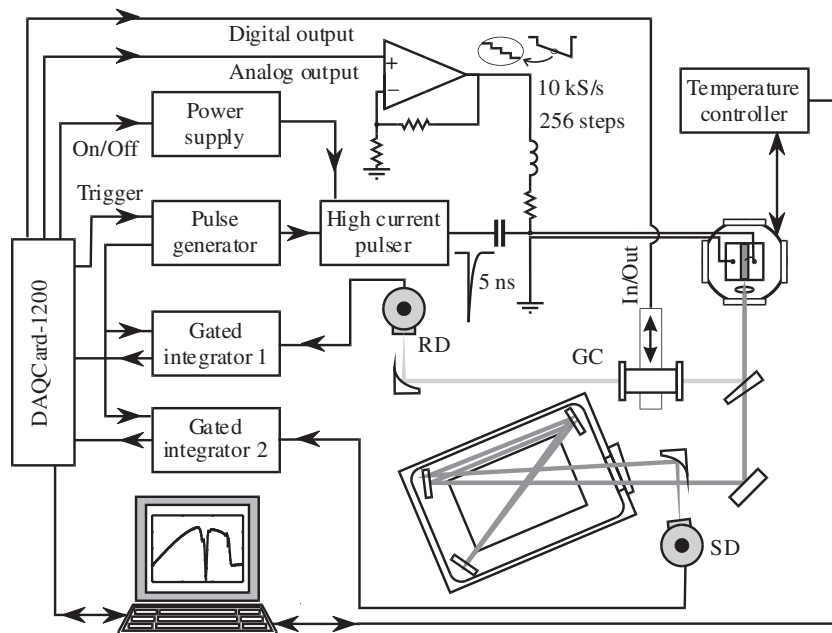


FIGURE 1 Schematic of QC-DFB laser based sensor for detection of biogenic carbon monoxide

The window of the vessel was uncoated, wedged  $\text{CaF}_2$  with a 25.4-mm diameter. The resulting path length inside the vessel was 102.5 cm and the total vessel volume was  $507 \text{ cm}^3$ . Both signal and reference beams were focused onto liquid nitrogen cooled HgCdTe detectors (signal and reference – SD and RD, respectively), each detector having a response time of 35 ns FWHM. The optical paths of the reference and signal beams outside of the vessel were matched in length to remove any effect of ambient atmospheric CO. A 3-cm-long gas cell (GC) shown in the reference beam contained 0.9% CO in a balance of air at 1-atm pressure and was mounted on a mechanical flipper controlled by a computer so that it could be automatically inserted into the reference beam path.

A high-current pulse generator module provided 5-ns-long,  $\sim 2$ -A-peak-current pulses to drive the QC-DFB laser at a repetition rate of 10 kHz. The laser used in this work generated IR radiation between  $2153$ – $2162 \text{ cm}^{-1}$  over a temperature range of  $+15 \text{ }^\circ\text{C}$  to  $-50 \text{ }^\circ\text{C}$  ( $-0.14 \text{ cm}^{-1}/^\circ\text{C}$  temperature-tuning coefficient). This wavelength range permitted access to the  $R(2)$ ,  $R(3)$ , and  $R(4)$  transitions in the CO fundamental vibration–rotation band. The  $R(3)$  line at  $2158.300 \text{ cm}^{-1}$  was chosen for the present experiments because it exhibited the smallest overlap with neighboring water-absorption lines. For this wavelength, the laser was operated at  $-22.6 \text{ }^\circ\text{C}$ .

Repetitive laser-frequency scans were performed according to the procedure described in [9, 10]. Briefly, a periodically modulated sub-threshold current ( $< 0.2 \text{ A}$ ) was supplied to the laser in addition to the nanosecond pulses and resulted in laser-frequency sweeps because of the Joule heating of the active area. The modulating waveform was digitally synthesized as an array of 256 numbers and converted to an analog output voltage, which was applied to the laser after the power amplifier. The digital/analog (D/A) conversion was synchronous with the nanosecond current pulses. Hence, each frequency scan consisted of 256 laser pulses. We applied a trapezoid wave (Fig. 2) to the power-amplifier input that resulted in an almost linear frequency scan of  $\sim 1 \text{ cm}^{-1}$ .

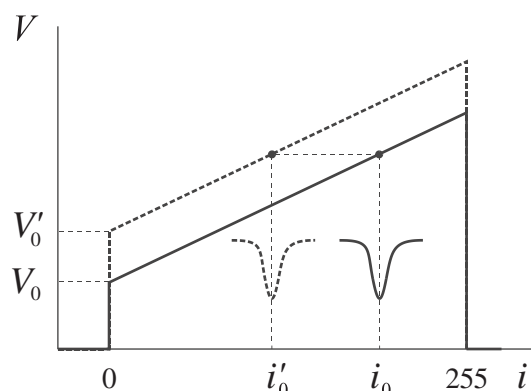


FIGURE 2 Principle of the laser-frequency stabilization by means of the digital feedback loop. When the offset voltage is changed from  $V_0$  to  $V'_0$ , the absorption-line position on the frequency scan moves from  $i_0$  to  $i'_0$

This scan length was estimated to be the minimum required to obtain reliable baseline identification in the vicinity of a pressure-broadened  $R(3)$  line with FWHM of  $0.13 \text{ cm}^{-1}$ . The laser substrate temperature was maintained at nominal  $T = -22.6 \text{ }^\circ\text{C}$  by the temperature controller. However, the temperature exhibited slow drifts during measurement runs of 10–50 h. This drift resulted in laser-frequency instability. A computer feedback loop was used in order to suppress this effect and is described in detail in Sect. 3.

Each laser pulse was synchronously detected by SD and RD, measured using two gated integrators (GIs) with a  $\sim 15$ -ns integration window, and subsequently digitized and stored on a laptop computer for further processing. The scans were repeated every 100 ms, limited by the time required to preprocess and store the data.

### 3 Experimental procedure

Rat aortic smooth muscle cells were selected as the subject. They were cultured and treated according to proced-

ures published in detail in [7]. Briefly, the cells were propagated in minimum essential medium until they reached confluence of  $\sim 10^7$  cells per flask, wherein the culture medium was replaced with a serum-free medium containing bovine serum albumin for 24 h. The cells were then treated with the heme oxygenase inducers, sodium nitroprusside (SNP; 1 mM) and hemin (20  $\mu$ M), and allowed to incubate for an additional 24 h prior to CO production rate measurements.

The vessel containing the cell-culture flask was equipped with two on-off valves to control the gas flow. For normal physiological activity, the cultures required an environment of air enriched with CO<sub>2</sub> to 5% concentration in order to maintain the pH of the medium. The vessel was ventilated with this air mixture prior to the measurements. The valves were closed during measurements of the endogenous CO production rate. The CO<sub>2</sub>-enriched air also contained trace background CO contamination at a concentration of  $\sim 400$  ppb, close to the average CO concentration in ambient air. We chose not to use any CO scrubbing filters to avoid an undesirable influence of the CO absorption-desorption processes on the measurements. Carbon monoxide production by the cells was measured as a change from this background concentration.

We identified several potential sources of uncertainty in the CO concentration measurements:

- 1) Pulse-to-pulse laser-energy fluctuations.
- 2) A slowly drifting offset in the output of each of the two GIs.
- 3) Interference fringes from optical elements, including the IR-detector windows.
- 4) Background CO and water (a weak absorption line at  $2158.105\text{ cm}^{-1}$  resulted in 0.07% absorption at 1-m path length in a saturated atmosphere of 45 Torr at  $+36\text{ }^\circ\text{C}$ ).
- 5) Slow laser-frequency drift caused by imperfect temperature stabilization.
- 6) GI noise of 2.5 mV, which introduced an error of  $\geq 0.25\%$  for each pulse when the detector signal was kept within the linear range of  $\leq 1\text{ V}$ .

In our sensor design, source (1) was excluded by two-channel detection with subsequent normalization, which also took into account GI offsets (source (2)). Background absorption and interference fringes (sources (3) and (4)) were considered as a baseline and removed by the subsequent data processing, as described in Sect. 4. Source (5) was eliminated by active laser-frequency stabilization via a digital feedback loop. The statistical error introduced by source (6) can only be reduced by averaging a large number of measurements.

The data-acquisition sequence consisted of the following steps:

1. Laser-frequency adjustment. A reference GC was inserted into the reference beam and a small number of scans (usually 50) was acquired. The CO absorption line peak position  $i_0$  was determined, and if it deviated from the initially established position by more than one point, a correction to the parameter  $V_0$  was made (Fig. 2). The laser-frequency scan is due to heating of the active region by the sub-threshold current. Therefore, an increase of  $V_0$  shifts the absorption line closer to the scan origin.

2. Data acquisition. The GC was removed from the beam and the data acquired and averaged over 600 scans, which took one minute. It yielded two arrays each of 256 numbers:  $S_n(i)$ ,  $n = 1, 2$  for the SD and RD, respectively, with  $i = 0 - 255$  as a laser-pulse index within each scan.
3. Offset measurement. The nanosecond current pulses were turned off and the GI offset for each channel was measured, averaged over 100 scans. The result was two numbers  $D_n$ ,  $n = 1, 2$  for SD and RD, respectively.
4. Preprocessing. The ratio  $R(i) = [S_1(i) - D_1]/[S_2(i) - D_2]$  was calculated and stored on a hard drive for further analysis. The reason for not determining the CO concentration in real time was that we explored various approaches to the data analysis. Once the best approach is established, it can be readily implemented in the software for real-time CO monitoring.

This sequence was automatically performed and repeated every 4.5 min. A result was a succession of files containing the absorption data  $R_t(i)$  as a function of time  $t$ . The data runs were performed with the opened vessel (ambient air), sealed vessel without live cells, and sealed vessel with a cell culture inside. Figure 3a presents an example of raw data collected from SD and RD (averaged over 600 scans) and the corresponding  $R(i)$ . The nonzero background slope in the  $R(i)$  trace

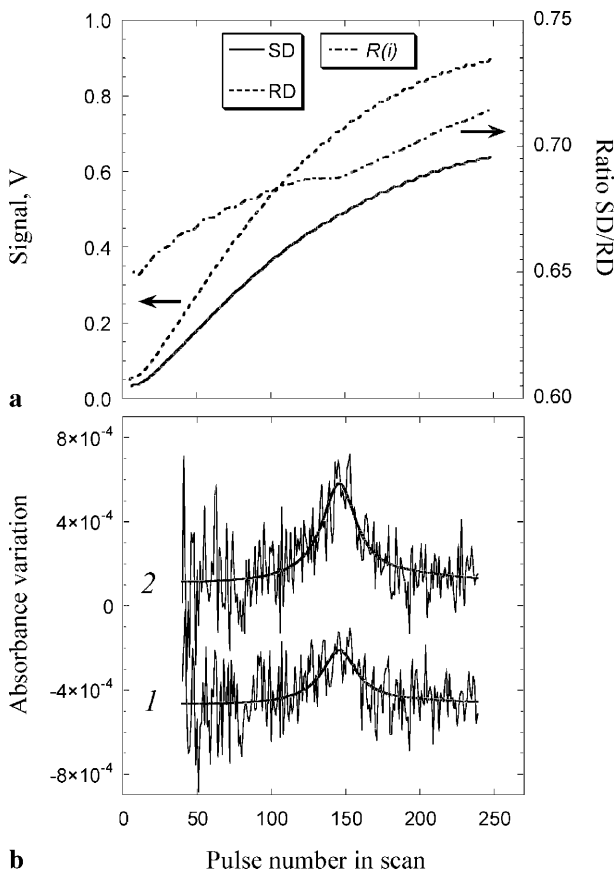


**FIGURE 3** **a** An example of the data collected after one sequence of measurements: 600 scans averaged, dc offsets subtracted from SD and RD data, and the ratio  $R(i)$  calculated. **b** Two examples of the difference spectra obtained from the  $R_t(i)$  succession. Best fit of spectra 1 and 2 yielded changes of atmospheric CO concentration of 94 ppb and 172 ppb, respectively

arises from interference effects that differ between the signal and reference paths and slightly nonlinear response of the detectors. In this run of measurements the vessel lid was opened and so the ambient air was investigated. The CO absorption can be noticed in the scan center, but the baseline is uncertain because of interference fringes having different periods. Concentration cannot be accurately determined from these data. However, if the laser-frequency scan always covers the same frequency range, then the deviations from the initially acquired data will reflect the CO concentration variations.

#### 4 Data analysis

In order to observe CO concentration changes in the vessel, an arbitrary data file from the succession  $R_t(i)$  was initially selected as a basic  $R_0(i)$ . A deviation from  $R_0(i)$  was considered as a linear combination of the three terms:

$$R_t(i) - R_0(i) = A_1 + A_2 \times (i - i_0) + A_3 \times L(i) \quad (1)$$

The first two terms are not related to the variations of CO concentration.  $A_1$  represents a deviation in SD/RD signal ratio from the initial value caused by the alignment drift and, in the experiments with the cell cultures, also by water condensation on the vessel window. A linear term with the  $A_2$  coefficient is introduced to provide a first-order compensation for a baseline distortion during the measurement runs. This distortion is due in part to the nonlinear response of the detectors, and therefore  $A_2$  exhibits a certain correlation with  $A_1$ . However, there were other sources of baseline instability such as temperature fluctuations in the photodetectors and small, temperature-dependent changes in the optical configuration.  $L(i)$  describes the absorbance of the CO sample with the known concentration  $[\text{CO}]_0$  acquired under the same conditions. We have acquired  $L(i)$  using the same GC with 0.9% CO as for the laser-frequency stabilization.  $i_0$  is a position of the maximum of the  $L(i)$  function. Two examples of the  $R_t(i) - R_0(i)$  data sets along with the best-fit curves described by (1) are shown in Fig. 3b.

A CO concentration deviation  $\Delta[\text{CO}]$  from the basic value will cause an additional attenuation of the main beam  $\alpha(i)$ , and

$$\frac{\Delta[\text{CO}]}{[\text{CO}]_0} = \frac{\alpha(i)}{L(i)} \quad (2)$$

For the ratio  $R_t$  of the signals from SD and RD we have

$$R_t = \frac{S_1}{S_2} = \frac{S'_1 - \alpha S'_1}{S_2} = R'_t - \alpha R'_t \quad (3)$$

where  $S'_1$  represents the main channel signal when  $\Delta[\text{CO}] = 0$  and  $R'_t = R_0(i) + A_1 + A_2(i - i_0)$ ;  $R'_t \approx R_0(i_0) + A_1$  in the vicinity of an absorption line centered at  $i_0$ . From (1), (2), and (3), we obtain

$$\alpha = \frac{R'_t - R_t}{R'_t} \approx \frac{A_3 L(i)}{R_0(i_0) + A_1} \quad (4)$$

and

$$\Delta[\text{CO}] = [\text{CO}]_0 \frac{A_3}{R_0(i_0) + A_1} \quad (5)$$

where  $[\text{CO}]_0$  is a concentration corresponding to the  $L(i)$  spectrum.

## 5 Results and discussion

We performed measurements of CO concentration variations in ambient air as an initial test of the CO sensor by removing the top of the flask container. The results of this sequence are shown in Fig. 4. The peak CO concentration exceeding 3000 ppb above the average was caused by exhaust emissions from heavy equipment associated with road-construction work just outside the laboratory building. The missing data sets near noon are a result of an instrument checkout resulting from the unexpectedly high levels of reported CO (the instrument was found to be operating properly). Short-term variations in the measured concentration are  $\sim 20$  ppb. Although these measurements do not provide the absolute CO concentration data, they show that the experimental and data analysis approach described here can also be used to create a short-open-path atmospheric CO monitor. The lowest absolute CO level in Fig. 4 is most probably 200–300 ppb, based on the results of previous work [11].

Another run of measurements was carried out with the cell culture prepared as described above. The results are shown in Fig. 5 along with the control run when the air sample was locked in the vessel without the cell culture. A gap in data between the sixth and seventh hours of the experiment was caused by water condensation on the inside surface of the vessel window. This problem can be eliminated by heating the window to  $\sim 38^\circ\text{C}$ . The data show a steady CO production rate of 44 ppb/h observed after  $\sim 2$  h of the initial setting time. Taking into account the 0.5-L volume of the vessel, this corresponds to a net CO production rate of  $0.9 \text{ nmol}/10^7 \text{ cells/h}$ , which is in reasonable agreement with previous measurements obtained with similar cells and treatment regimens [7]. The initially high CO production rate for the first two hours of the experiment may be due to outgassing of CO from the cell-culture medium or temperature stabilization of the cells from the laboratory air to the warmer ( $37^\circ\text{C}$ ) temperature of the measurement chamber.

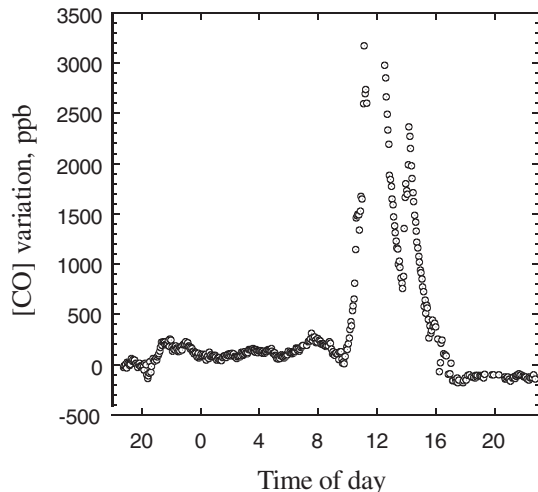


**FIGURE 4** Observed evolution of CO concentration in ambient air during a  $\sim 24$ -h time interval for 1-m open path length measurements

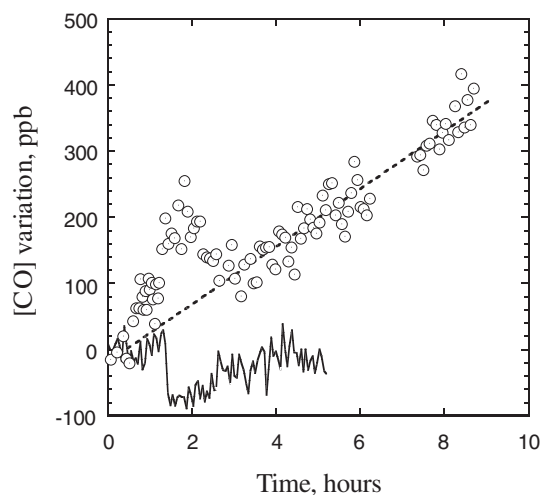


**FIGURE 5** Results of CO concentration measurements in the sealed vessel: *solid line*, control experiment, no cell culture inside the vessel; *circles*, a similar experiment with cell culture inside. *Dashed line*, best linear fit of data, first three hours are excluded. The fit shows a CO production rate of 44 ppb/h

## 6 Conclusion

We demonstrated the first application of a pulsed QC-DFB laser to in vitro monitoring of live cell-culture activity through the measurements of CO production rate. The limiting sources of uncertainty in the present setup are the GI noise and optical alignment drift. The first, statistical, error will be reduced with a larger number of laser pulses involved in each measurement or with a higher-performance GI. We are presently upgrading the laser pulser and data-acquisition system from 10-kHz repetition rate used in this work to 1-MHz repetition rate. This should decrease the statistical error 10 times for the same data-acquisition time. The second error source can be eliminated only by a better (more stable) optomechanical design and thermal stabilization.

It was also shown that monitoring of the atmospheric CO can be performed using basically the same technique and a 1-m open path length. This task is actually easier because it does not require a special artificial environment as for the cell culture, and also the CO concentration varies more noticeably. Assuming a rugged mechanical construction, the described configuration requires only a one-time calibration to provide absolute data for CO concentration in air.

**ACKNOWLEDGEMENTS** Financial support of the work performed by the Rice group and PSI was provided by NIH through Grant No. 1R43HL64452-02-01A1. Rice also acknowledges support from the National Aeronautics and Space Administration (NASA), the Institute for Space Systems Operations (ISSO), the Texas Advanced Technology Program, the National Science Foundation, and the Welch Foundation. The work performed at Baylor College of Medicine was supported by the National Heart, Lung, and Blood Institute through Grant No. HL 59976 and an Established Investigator Grant from the American Heart Association. The work performed at Bell Laboratories was partly supported by DARPA/US ARO under Contract No. DAAD19-00-C-0096. R. Köhler acknowledges support from the Deutsche Studienstiftung.

## REFERENCES

- 1 N. Christodoulides, W. Durante, M.H. Kroll, A.I. Schafer: *Circulation* **91**, 2306 (1995)
- 2 T. Ingi, J. Cheng, G.V. Ronnett: *Neuron* **16**, 835 (1996)
- 3 M.N. Cook, K. Nakatsu, G.S. Marks, B.E. McLaughlin, H.J. Vreman, D.K. Stevenson, J.F. Brien: *Can. J. Physiol. Pharmacol.* **73**, 515 (1995)
- 4 L. Grundemar, M.B. Johansson, M. Ekelund, E.D. Hogestatt: *Acta Physiol. Scand.* **153**, 203 (1995)
- 5 F.W. Sunderman, Jr., J.R. Downs, M.C. Reid, L.M. Bibeau: *Clin. Chem.* **28**, 2026 (1982)
- 6 T. Ingi, J. Cheng, G.V. Ronnett: *Neuron* **16**, 835 (1996)
- 7 Y. Morimoto, W. Durante, D.G. Lancaster, J. Klattenhoff, F.K. Tittel: *Am. J. Physiol. Heart Circ. Physiol.* **280**, H483 (2001)
- 8 R. Köhler, C. Gmachl, A. Tredicucci, F. Capasso, D.L. Sivco, S.N.G. Chu, A.Y. Cho: *Appl. Phys. Lett.* **76**, 1092 (2000)
- 9 A.A. Kosterev, F.K. Tittel, C. Gmachl, F. Capasso, D.L. Sivco, J.N. Bailargeon, A.L. Hutchinson, A.Y. Cho: *Appl. Opt.* **39**, 6866 (2000)
- 10 A.A. Kosterev, F.K. Tittel, R.F. Curl, R. Köhler, C. Gmachl, F. Capasso, D.L. Sivco, A.Y. Cho: *Appl. Opt.* (2002) to appear
- 11 A.A. Kosterev, F.K. Tittel, R. Köhler, C. Gmachl, F. Capasso, D.L. Sivco, A.Y. Cho, S. Wehe, M. Allen: *Appl. Opt.* (2002) to appear